HOKKAIDO UNIVERSITY

Title	Immunolocalization of sclerostin synthesized by osteocytes in relation to bone remodeling in the interradicular septa of ovariectomized rats
Author(s)	Guo, Ying; Li, Minqi; Liu, Zhusheng; Yamada, Tamaki; Sasaki, Muneteru; Hasegawa, Tomoka; Hongo, Hiromi; Tabata, Chihiro; Suzuki, Reiko; Oda, Kimimitsu; Yamamoto, Tsuneyuki; Kawanami, Masamitsu; Amizuka, Norio
Citation	Journal of Electron Microscopy, 61(5), 309-320 https://doi.org/10.1093/jmicro/dfs052
Issue Date	2012-10
Doc URL	http://hdl.handle.net/2115/52954
Rights	This is a pre-copy-editing, author-produced PDF of an article accepted for publication in Journal of Electron Microscopy following peer review. The definitive publisher-authenticated version J Electron Microsc (Tokyo) (2012) 61 (5): 309-320 is available online at: http://jmicro.oxfordjournals.org/content/61/5/309
Type	article (author version)
File Information	JEM61-5_309-320.pdf

Instructions for use

Hokkaido University Collection of Scholarly and Academic Papers : HUSCAP

Immunolocalization of sclerostin synthesized by osteocytes in relation to bone remodeling in the interradicular septa of ovariectomized rats

Ying Guo[1,2], Minqi Li[1,3], Liu Zhusheng[1], Muneteru Sasaki[1], Tomoka Hasegawa[1], Hiromi Hongo[1,2], Chihiro Tabata[1], Reiko Suzuki[1], Kimimitsu Oda[3], Tsuneyuki Yamamoto[1], Masamitsu Kawanami[2], Norio Amizuka[1]

Departments of [1]Developmental Biology of Hard Tissue, and [2]Periodontology and Endodontology, Graduate School of Dental Medicine, Hokkaido University, Sapporo, Japan
[3]Shandong Provincial Key Laboratory of Oral Biomedicine, The School of Stomatology, Shandong University, Jinan, China
[4]Division of Biochemistry, Niigata University Graduate School of Medical and Dental Sciences, Niigata, Japan

Running title: ***sclerostin synthesis in OVX***

Address for correspondence:

Norio Amizuka, DDS, PhD
Department of Developmental Biology of Hard Tissue
Graduate School of Dental Medicine
Hokkaido University
Kita 13 Nishi 7 Kita-ku
Sapporo, 060-8586, Japan
Tel: +81-11-706-4223
Fax: +81-11-706-4226
E-mail: amizuka@den.hokudai.ac.jp

ABSTRACT

This study aimed to elucidate whether estrogen deficiency would affect the synthesis of an osteocyte-derived factor, sclerostin, in the mesial region of alveolar bone. Eight 9-week-old Wister female rats were ovariectomized (OVX), and the other eight rats were Sham-operated (Sham). After 4 weeks, the interradicular septa of mandibular first molar were embedded in paraffin, and then, were histochemically examined. Sclerostin-positive osteocytes were located in a superficial layer of the mesial region of Sham bone, while the OVX mesial region showed a lesser presence of the sclerostin-reactive osteocytes. There was no significant difference in the distribution of estrogen receptor α and TUNEL-positive cells in either Sham or OVX groups. Meanwhile, the Sham mesial region demonstrated many osteoclasts, but the OVX specimens showed numerous osteoclasts in association with intense immunolabeling of the receptor activator of the nuclear factor kB ligand. Complex meshwork of cement lines was seen consistent with irregularly-distributed osteocytic lacunar-canalicular system in the OVX mesial region, compared with those of the Sham specimens. In conclusion, estrogen deficiency appears to inhibit osteocytes for sclerostin synthesis in the mesial region of the interradicular septum, mediated by accelerated bone remodeling, rather than by directly effecting osteocytes.

193 words

Key words: ovariectomy, osteocyte, sclerostin, estrogen receptor α, alveolar bone

INTRODUCTION

Osteocytes are localized within their lacunae, and are connected to each other by means of their cytoplasmic processes through gap junctions [1, 2]. Osteocytes' cytoplasmic processes run through narrow passageways referred to as osteocytic canaliculi, and build up functional syncytia, *i.e.*, the osteocytic lacunar-canalicular system (OLCS) [3-5]. OLCS have been shown to sense the direction and strength of mechanical stress in bone, and then, affect the communication among osteocytes and between osteocytes and osteoblasts [4,6,7]. Alveolar bone, which forms the tooth socket surrounding the roots of teeth, has unique histological properties harmonized with mechanical stress. In rat mandibles, the physiological distal movement of the molars causes continuous bone resorption and bone formation on the mesial and distal regions of the interradicular septum, due to compression and tensile forces. Although osteocytes in the alveolar bone might sense such mechanical stress and affect bone metabolism, this is still an on-going investigation since mechanical stress is difficult to detect. Nevertheless, it seems of importance to examine the mesial region of the interradicular septum in order to elucidate the osteocytic function related to bone resorption bearing physiological force.

Osteocyte-derived molecules were recently highlighted because the synthesis of these molecules may reflect osteocytic function responding to mechanosensing, regulation of bone remodeling and so forth. Dentin matrix protein-1 (DMP-1) has been shown to be a bone matrix protein expressed in osteocytes, and has been assumed to play a pivotal role in bone mineral homeostasis, due to its high calcium-binding affinity [8,9]. Another osteocyte-derived factor, sclerostin, is a glycoprotein encoded by the *SOST* gene [10], and was reported to bind the LRP5/6 receptor, thereby antagonizing Wnt signaling and increasing β-catenin degradation [11,12]. Sclerostin has been reported as a negative regulator of osteoblastic bone formation [12-15]: Sclerostin secreted by osteocytes may pass through the

osteocytic canaliculi and inhibit bone-lining osteoblasts. Taken together, osteocytes are not merely resting cells embedded in bone, but appear to be dynamically related to bone metabolism, *e.g.*, by secreting sclerostin.

It is well known that patients suffering from post-menopausal osteoporosis, *i.e.*, estrogen deficiency, show stimulated osteoclastic bone resorption. Likely, alveolar bone showed an increased remodeling [16-21], a decrease in bone volume of the mandible [22] and cancellous bone loss in the mandibular condyle [23]. The estrogen deficiency-induced osteoporosis appears to be a result of the binding of the receptor activator of the nuclear factor κB (RANK) and RANK ligand (RANKL), as previously reported [24-26]. RANK is a member of the membrane-associated tumor necrosis factor receptor family located on cell membranes of osteoclasts and their precursors [27,28], while RANKL is present on the cell membrane of osteoblast lineages [27-29]. Recently, Masuki *et al* [30] reported that osteocytic synthesis of sclerostin was markedly inhibited in long bones of mice lacking osteoprotegerin, a decoy receptor for RANKL inhibiting osteoclastogenesis [31], and therefore, it seems likely that osteocytes are influenced by estrogen deficiency-induced osteoporosis.

Estrogen deficiency may directly affect osteocytes, because they have been shown to possess the estrogen receptors (ERs) [32]. Two ERs have been identified: α and β, which are distinct proteins encoded by separate genes located on different chromosomes. ERα consists of 595 amino acid residues with a molecular mass of 66 kDa [33], while ERβ consists of 485 amino acid residues with a molecular mass of 54 kDa [34], both of which have shown high homology of the amino acid sequence. Braidman *et al.* reported that ERα among these receptors was expressed in human osteoblasts, and resultant ERα protein was detected in osteocytes, indicating that ERα is a major receptor in osteocytes [35]. Therefore, it seems of importance to elucidate whether estrogen deficiency would affect osteocytes by mediating accelerated bone resorption or by a direct effect through their receptors.

In this study, we have attempted to elucidate whether estrogen deficiency would affect the immunolocalization of sclerostin, an osteocyte-derived factor regulating bone remodeling, by examining the mesial region of the interradicular septum in ovariectomized rats, which are subjected to continuous bone resorption. In addition, we attempted to provide histological clues for understanding how estrogen deficiency affects osteocytes on the sclerostin synthesis.

MATERIALS AND METHODS

Animals and Tissue preparation

Nine-week-old female Wister rats (Japan CLEA, Tokyo, Japan) were used in the experiments for the Sham operation (Sham group, n=8) and ovariectomy (OVX group, n=8) under anesthesia with an intraperitoneal injection of chloral hydrate, which followed the Guiding Principles for the Care and Use of Animals approved by Hokkaido University (No.10-0059). After 4 weeks, the rats of both the Sham and OVX groups were perfused through the left ventricle with 4% paraformaldehyde solution diluted in 0.1 M cacodylate buffer (pH 7.4). Mandibles were removed and immersed with the same fixative for 12 h at 4 °C. Samples were decalcified with 10% ethylenediamine tetraacetic disodium salt (EDTA-2Na) solution. The decalcified specimens were dehydrated in ascending alcohol prior to paraffin embedding. Histological sections of the mandibles were obtained by sectioning in an assumed sagittal plain including proximal and lingual distal roots of the first molar. Specimens were observed under a Nikon Eclipse E800 microscope (Nikon Instruments Inc. Tokyo, Japan). Light microscopy images were acquired with a digital camera (Nikon DXM1200C, Nikon).

Enzyme histochemistry for tartrate-resistant acid phosphatase (TRAP), and immunohistochemistry for sclerostin, DMP-1, ERα, osteopontin and RANKL

Tartrate-resistant acid phosphatase (TRAP) was detected as previously described [36]; briefly, deparaffinized sections were rinsed with phosphate-buffered saline (PBS) and incubated in a mixture of 2.5 mg of naphthol AS-BI phosphate (Sigma, St. Louis, MO), 18 mg of red violet LB (Sigma) salt and 100 mM L (+) tartaric acid (0.76 g) diluted in 30 mL of 0.1M sodium acetate buffer (pH 5.0) for 15 min at 37 °C.

For immunohistochemistry, dewaxed paraffin sections were used for detection of sclerostin, DMP-1 and osteopontin as previously reported [30,37]. Endogenous peroxidase

inhibition was conducted for all sections, and that was the first step in staining unless otherwise stated. For DMP-1 detection, sections were treated with 1μg/mL trypsin (Wako Pure Chemical Industries Ltd., Osaka, Japan) for 30 min prior to inhibition of endogenous peroxidase activity. After pre-incubation with 1% bovine serum albumin diluted in PBS (BSA-PBS) for 30 min at room temperature, sections were incubated with rabbit antibody against DMP-1 (Takara Bio Inc., Otsu, Japan) at a dilution of 1: 500 overnight at 4 °C. As with osteopontin detection, the sections were incubated with rabbit anti-osteopontin antisera (Cosmo Bio, Co., Ltd., Tokyo, Japan) for 1 h. For sclerostin detection, the sections were incubated with goat anti-sclerostin (R&D System Inc., Minneapolis, MN) at a dilution of 1:100. These sections were subsequently reacted with horseradish peroxidase (HRP)-conjugated anti-rabbit IgG (for DMP-1 and osteopontin; DakoCytomation, Glostrup Denmark) or HRP-conjugated anti-goat IgG (for sclerostin; American Qualex, San Clemente, CA) at 1:100 at room temperature. As with immunodetection of RANKL, the histological sections treated with 1% BSA-PBS were incubated with rat antibody against mouse RANKL (Oriental Yeast Co., Ltd, Tokyo, Japan) at a dilution of 1: 50, and then, reacted with HRP-conjugated anti-rat IgG (Zymed laboratories Inc., South San Francisco, CA). Regarding immunochemistry of estrogen receptor α, ERα, the dewaxed paraffin sections were immersed in a solution of 0.01 M Tris-EDTA buffer (pH 9.0) with 0.05% Tween-20 at 65 °C in water bath for 30 min. Thereafter, they were rinsed with 0.05M Tris-HCl (pH 7.6) supplemented with 1% Tween-20 (washing buffer) for 5 min at room temperature. The sections were incubated with rabbit antibody to ERα (DB Biotech, Kosice, Slovak Republic) at a dilution of 1: 100 with the washing buffer for 2 h. After rinsing with the washing buffer, the sections were treated with HRP-conjugated anti-rabbit IgG (DakoCytomation) at a dilution of 1: 100 for 1 h at room temperature.

For visualization of all immunoreactions, diaminobenzidine (DAB) tetrahydrochloride was employed as a substrate. All sections were counterstained faintly with hematoxylene or

methyl green, and observed under a light microscope (Eclipse E800, Nikon Instruments Inc. Tokyo, Japan).

Double staining of ERα and cathepsin K, and triple detection of alkaline phosphatase (ALP), TRAP and sclerostin

Regarding double immunostaining for ERα and cathepsin K, the sections were subjected to ERα detection as described above. They were, then, incubated with mouse anti-human cathepsin K (Daiichi Fine Chemical. Co., Ltd., Toyama, Japan) at a dilution of 1: 200 with 1% BSA-PBS for 2 h at room temperature, followed by incubation with alkaline phosphatase (ALP)-conjugated anti-mouse IgG (Jackson ImmunoResearch Laboratories, Inc., PA). For visualizing ALP enzyme activity, the treated sections were dipped in a mixture of 2.5 mg of naphthol AS-BI phosphate (Sigma) and 18 mg of fast blue RR salt (Sigma) diluted in 30 ml of 0.1M Tris-HCl buffer (pH 8.5) at 37 °C for 30 min. For triple staining of sclerostin, ALP and TRAP, sclerostin-immunoreactivity was first visualized by DAB reaction. Subsequently, the sections were incubated with rabbit anti-tissue nonspecific ALP [38] at a dilution of 1: 200, following the incubation with ALP-conjugated anti-rabbit IgG (Jackson ImmunoResearch Laboratories) at a dilution of 1: 100 at room temperature. Finally, TRAP detection was conducted on the sclerostin/ALP-labeled sections, as described above.

Silver impregnation

Silver impregnation was performed as previously described [39]. Dewaxed sections were soaked in a 1.5% Protargol-S solution diluted in borax-boric acid (pH 7.4) for 40 h at 37 ^{o}C. After rinsing in distilled water, the reaction was enhanced by an aqueous solution containing 0.2% hydroquinone, 0.2% citric acid and 0.7% nitric silver. After additional rinsing, the sections were reacted for 5 min with a solution of 2.5 % anhydrous sodium sulfite, 0.5% potassium bromide and 0.5% amidol diaminophenol dihydrochloride. They were then

treated with 1% gold chloride, and subsequently treated by 2% oxalic acid amidol until the osteocytic canaliculi were stained black.

Quantification of sclerostin-positive osteocytes in the mesial regions of the alveolar bone

In order to quantify the sclerostin-positive osteocytes in relation to the distance from the mesial bone surface, we made an assumed rectangle (240 μm in width, 1.2 mm in height), of which the longitudinal line overlapped the mesial surface of the alveolar bone, and evenly divided it into eight rectangles with 30μm in width. The total number of osteocytes and the number of sclerostin-positive osteocytes were counted in the assumed rectangles in the mesial region of the interradicular septum. Sclerostin-positive osteocytes were recognized with the aid of ImagePro Plus 6.2 software (Media Cybernetics, Silver Spring, MD), as previously reported [40,41]. The percentage of sclerostin-positive osteocytes in each rectangle was statistically analyzed between the Sham-operated and OVX specimens (n=8 per group).

Detection and Quantification of apoptotic cells positive for TUNEL

For detection of apoptotic cells in the specimens, the "TACS 2TdT-Blue Label In Situ Apoptosis Detection Kit" (Trevigen Inc., Gaithersburg, MD) for the terminal deoxynucleotidyl transferase-mediated deoxyuridinetriphosphate nick end-labeling (TUNEL) method was employed. Dewaxed sections were incubated with 1% proteinase K (Trevigen Inc.) diluted 1: 200 at 37 °C for 15 min, followed by inhibition of the endogenous peroxidases at room temperature for 5 min. After treatment with TdT enzyme at a dilution of 1: 50 at 37 °C for 1 h, sections were incubated with HRP-conjugated streptavidin at room temperature for 15 min. Reaction was made visible with the blue label solution provided in the kit. Quantification of TUNEL-positive cells was performed according to the method described in the quantification of sclerostin-positive osteocytes using an assumed rectangle (240 μm in width, 1.2 mm in height)

Statistical analysis

All statistical analyses were performed using Microsoft Excel 2003 Analysis ToolPak (Microsoft Corporation, Redmond, WA), and all values are presented as means ± standard deviation. Differences among groups were assessed by the unpaired Student's *t*-test, and considered statistically significant when $P < 0.05$.

RESULTS

Accelerated bone resorption and evenly-distributed DMP-1-positive osteocytes in the mesial region of the OVX interradicular septum

After 4 weeks of OVX, the mesial region of the interradicular septum of the first molar showed an increased population of TRAP-positive osteoclasts, in contrast with that of the Sham-operated specimens **(Figs. 1A, 1B)**. However, the distal region did not localize so many TRAP-reactive osteoclasts even in the OVX specimens. The interradicular septum showed the evenly-distributed immunoreactivity of DMP-1, a bone matrix protein expressed in osteocytes, throughout the septa in both the Sham-operated and OVX groups **(Figs. 1C, 1D)**. When observing the mesial region at a higher magnification, the intensity of DMP-1 immunoreactivity of osteocytes was similar between the Sham and OVX groups **(Figs. 1E, 1F)**. These findings imply that OVX accelerated the osteoclasts' accumulation in the mesial region and that DMP-1 synthesis is not affected by stimulated osteoclast bone resorption.

Reduced sclerostin-immunoreactivity in the mesial region of the OVX specimens

In Sham-operated specimens, triple staining of ALP, TRAP and sclerostin demonstrated little sclerostin in osteocytes closely neighboring the mesial surface, on which several TRAP-positive osteoclasts were localized **(Figs. 2A, 2C)**. In contrast, the mesial region of the OVX septa displayed more osteocytes lacking sclerostin-immunoreactivity **(Figs. 2B, 2E)**. In the corresponding area, many TRAP-positive osteoclasts and intense ALP-positive osteoblastic cells were seen accompanied with irregularly-resorbed bone surfaces **(Fig. 2E)**. Unlikely, in both the Sham-operated and OVX groups, the inner region of the interradicular septa had many osteocytes with sclerostin-positivity, and the distal regions lacked sclerostin-positive osteocytes merely in the superficial layer **(Compare Figs. 2D and 2F)**. In order to clarify the localization of sclerostin-negative osteocytes after OVX, we performed

statistical analysis on the quantification of the sclerostin-immunoreactive osteocytes in relation to the distance from the mesial surface **(Fig. 2G)**. In the Sham group, osteocytes very close to the mesial surface (up to 30μm in depth) did not reveal sclerostin-immunoreactivity. When observing the mesial surface toward the distal region, however, sclerostin-positive osteocytes were immediately discernible. In contrast, the OVX septa exhibited no sclerostin-positivity over a broad area, extending to 90 μm in depth from the mesial surface **(Fig. 2G)**. The innermost areas 90 to 240 μm distant from the mesial surfaces revealed sclerostin-positive osteocytes, with no significant difference in the index of sclerostin-positive osteocytes between the Sham-operated and OVX groups. Thus, triple histochemical staining and the statistical analysis verified the broad absence of sclerostin-positivity in the mesial region of the OVX interradicular septa.

Immunolocalization of ERα and TUNEL-positive osteocytes in the interradicular septa after the OVX

In order to provide clues to whether the reduced sclerostin in osteocytes was directly affected by ERα, we next examined immunolocalization of ERα/cathepsin K in the Sham and OVX groups. As a consequence, the ERα-immunopositivity was detected in the nuclei of osteoblasts, osteocytes and periodontal cells, as well as in cathepsin K-positive osteoclasts in the mesial and distal regions even after the OVX **(Fig. 3)**. Although ERα expression was reported to be reduced in long bones with OVX [42], there was no apparent difference in the distribution of ERα-positive osteocytes in the mesial regions of the Sham and OVX specimens **(Figs. 3E and 3F)**. Interestingly, not all osteocytes showed ERα-positivity, indicating heterogeneous expression of this receptor. Thus, reduced-sclerostin did not appear to be associated with diminished ERα in osteocytes in the mesial region. Other studies suggested a proapoptotic effect of estrogens on osteoclasts and osteoblasts [43,44], and therefore, it was necessary to confirm whether the reduced amount of sclerostin would be

related to an anti-apoptotic effect by estrogen deficiency. However, our histological examination showed the similar distribution of TUNEL-positive cells in the mesial and distal regions **(Figs. 3G-3J)**. Consistently, there was no significant difference in the index of TUNEL-positive cells between the Sham and OVX groups (3.28 ± 1.45 vs 2.41 ± 1.2, NS). Thus, the immunolocalization of ERα and apoptotic cells did not change in the OVX alveolar bone.

Increased immunoreactivity of RANKL in the periodontal ligament and complicated meshwork of cement lines in the mesial region of the OVX interradicular septa

Another possibility to reduce sclerostin synthesis in osteocytes appears to be involved in accelerated bone remodeling in the OVX specimens. Therefore, we next examined the immunoreactivity of RANKL, an essential factor for osteoclastogenesis, and as a consequence, OVX periodontal ligaments showed more intense immunolabeling for RANKL compared with that seen in the Sham specimens **(Figs. 4A, 4B)**. The deeper area of OVX mesial region showed complicated meshwork of TRAP-positive, and osteopontin-positive cement lines, a histological hallmark of bone remodeling, while Sham-specimens had several cement lines merely in the most superficial area **(Figs. 4C-4F)**. Therefore, OVX appeared to increase RANKL synthesis, which led to not only increased osteoclastic numbers but also active bone remodeling even in the deeper areas. In such areas featuring active bone remodeling, silver impregnation demonstrated the irregular distribution of the osteocytic lacunar-canalicular system, OLCS, in OVX specimen, while the Sham specimens had regular distribution of osteocytes and their canaliculi **(Figs. 4G, 4H)**. Taken togerther, it seems likely that accelerated bone remodeling in the OVX mesial region of the interradicular septum caused irregular distribution of osteocytes and their canaliculi.

DISCUSSION

To our knowledge, this is the first report to demonstrate *in vivo* immunolocalization of sclerostin, an osteocyte-derived factor regulating osteoblastic activity, in the alveolar bone with estrogen deficiency. Our study showed, in the mesial region of the OVX interradicular septum, 1) an increased number of osteoclasts and intense labeling of RANKL, an essential factor for osteoclastogenesis, 2) the broad absence of sclerostin-positive osteocytes, 3) no histological alteration of ERα immunoreactivity or apoptotic cells, and 4) stimulated bone remodeling and irregular distribution of OLCS. Literally, irregular OLCS caused by stimulated bone remodeling reduced the synthesis of sclerostin in long bones [30]. Therefore, accelerated bone remodeling induced by estrogen deficiency, rather than a direct effect through osteocytic ERα, appeared to inhibit sclerostin-positivity in osteocytes in the mesial region of the interradicular septa. This means that bone remodeling or its participating cells: osteoblasts and osteoclasts, would affect osteocytes for sclerostin synthesis, a new insight on the intercellular regulation - bone remodeling or participating cell-derived regulation of the sclerostin synthesis.

It is well known that OVX stimulates osteoclastic differentiation and subsequent bone resorption in long bones, and also shows the similar effects in alveolar bone [16-22]. Consistently, our immunohistochemistry revealed increased RANKL immunoreactivity in the OVX periodontal ligament including many TRAP-positive osteoclasts. However, as shown in **Fig. 1**, the distribution pattern of osteoclasts appeared to be unaltered even after OVX-mediated osteoclast differentiation. The compression force that is driven by physiological distal movement of teeth may accumulate osteoclasts on the mesial region after their promoted differentiation by estrogen deficiency. In addition, the complex meshwork of cement lines shown in **Fig. 4** implies active bone remodeling, *i.e.*, not only stimulated bone resorption, but also enhanced bone formation by osteoblasts in this region. Thus, the mesial

region of the interradicular septa appear to be an appropriate site for examining osteocytic function responding to physiological or stimulated bone remodeling in Sham-operated or OVX rats, respectively.

Our study demonstrated few sclerostin-immunoreactive osteocytes in the broad area of the mesial region in OVX rats, compared with that in the Sham group. Complex meshwork of cement lines broadly distributed in the OVX mesial region appeared to be in agreement with fragmented osteocytic lacunar-canalicular system, referred to as OLCS, in the corresponding region. Masuki *et al* demonstrated fragmented OLCS by stimulated bone remodeling in mice with osteoprotegerin-depletion, and markedly-reduced synthesis of sclerostin [30]. In our study, the estrogen deficiency induced intense reactivity of RANKL in the mesial region of the alveolar bone, which may provide a similar milieu for osteoclastogenesis as that reported by Masuki *et al*. Therefore, it seems reasonable that enhanced RANKL by estrogen deficiency would stimulate bone remodeling in the deeper mesial region, resulting in the fragmented OLCS, which inhibits secretion of sclerostin in osteocytes. One may wonder why irregular distribution of OLCS would lead to this type of inhibition. We hypothesized that geometrically regular distribution of OLCS would be functionally efficient for sensing the direction and the strength of mechanical force, and for recognizing cellular activity including bone remodeling. Co-incidently, we have also reported that there were few osteocytes expressing fibroblast growth factor 23, an osteocyte-derived factor regulating serum concentration of phosphate, in the metaphyseal primary trabecules, in which osteocytes were randomly distributed in the irregular canaliculi [39]. Taken together, reduced synthesis of sclerostin in osteocytes appears to be related to actively-remodeled bone featuring irregularly-distributed OLCS.

However, this may raise the question of whether estrogen deficiency would first inhibit the osteocytic synthesis of sclerostin, and thereafter, the reduced synthesis of sclerostin would permit accelerated osteoblastic bone formation and bone remodeling. In order to answer this

question, we examined the immunolocalization of the estrogen receptor, ERα, which is a major ER [35], since Lim *et al.* demonstrated extremely-reduced expression of ERs in cancellous bone after OVX [42]. However, our histochemical study demonstrated no obvious difference in the ERα-immunoreactivity in the osteocytes' nuclei of Sham-operated and OVX specimens. This implies that reduced sclerostin was not associated with diminished ERα in osteocytes in the mesial region. But, there still remains the possibility that signaling linked to ERα would be altered even though the immunolocalization of ERα was unchanged. Recently, the proapoptotic effect of estrogens on osteoclasts was reported to be mediated by an increase in Fas ligand production by osteoclasts [44], and *in vitro* studies showed that estrogens stimulate Fas ligand expression in osteoblastic cells which are precusors of osteocytes [43]. However, we showed no obvious difference in the number of TUNEL-positive osteoblasts and osteocytes even after the OVX. Therefore, it seems likely that reduced sclerostin in osteocytes is not related to signaling linked to anti-apoptosis by estrogen. In addition, the idea that estrogen deficiency directly reduces sclerostin in all osteocytes could not explain why only osteocytes in the mesial region decreased to synthesize sclerostin. Therefore, it seems reasonable to consider that the local circumstances such as accelerated bone remodeling resulted in the attenuated sclerostin in the mesial region. Taken all together, it seems likely that bone remodeling rather than the direct effect mediated by ERα would affect the immunolocalization of sclerostin in osteocytes in the mesial region of the interradicular septum.

CONCLUDING REMARKS

We have demonstrated that estrogen deficiency inhibited sclerostin-synthesis in osteocytes broadly distributed in the mesial region of interradicular alveolar bone, and also provided clues for histological mechanisms in reducing sclerostin-synthesis, which appeared to mediate increased RANKL and consequent stimulated bone remodeling in the corresponding area.

Acknowledgement

This study was partially supported by grants from the Japanese Society for the Promotion of Science (Amizuka N, Li M, Suzuki R).

REFERENCES

1. Doty SB (1981) Morphological evidence of gap junctions between bone cells. *Calcif. Tissue Int.* **33**: 509-512.

2. Shapiro F (1997) Variable conformation of GAP junctions linking bone cells: a transmission electron microscopic study of linear stacked linear, curvilinear, oval, and annular junctions. *Calcif .Tissue Int.* **61**: 285-293.

3. Aarden EM, Burger EH , and Nijweide PJ (1994) Function of osteocytes in bone. *J .Cell. Biochem* .**55**: 287-299.

4. Burger EH , and Klein-Nulend J (1999) Mechanotransduction in bone role of the lacuno-canalicular network. *FASEB J.* **13**:101-112.

5. Knothe Tate ML, Adamson JR, Tami AE , and Bauer TW (2004) The osteocyte. *Int .J. Biochem .Cell Biol.* **36**:1-8.

6. Klein-Nulend J, van der Plas A, Semeins CM, Ajubi NE, Frangos JA, Nijweide PJ , and Burger EH (1995) Sensitivity of osteocytes to biomechanical stress in vitro. *FASEB J* .**9**:441-445.

7. Weinbaum S, Cowin SC , and Zeng Y (1994) A model for the excitation of osteocytes by mechanical loading-induced bone fluid shear stresses. *J. Biomech.* **27**: 339-360.

8. George A, Gui J, Jenkins NA, Gilbert DJ, Copeland NG , and Veis A (1994) In situ localization and chromosomal mapping of the AG1 (Dmp1) gene. *J. Histochem .Cytochem.***42**:1527-1531.

9. Toyosawa S, Shintani S, Fujiwara T, Ooshima T, Sato A, Ijuhin N , and Komori T (2001) Dentin matrix protein 1 is predominantly expressed in chicken and rat osteocytes but not in osteoblasts. *J .Bone Miner .Res.* **16**: 2017-2026.

10. Winkler DG, Sutherland MK, Geoghegan JC, Yu C, Hayes T, Skonier JE, Shpektor D, Jonas M, Kovacevich BR, Staehling-Hampton K, Appleby M, Brunkow ME , and Latham JA (2003) Osteocyte control of bone formation via sclerostin, a novel BMP antagonist. *EMBO J* .**22**: 6267-6276.

11. Li X, Zhang Y, Kang H, Liu W, Liu P, Zhang J, Harris SE , and Wu D (2005) Sclerostin binds to LRP5/6 and antagonizes canonical Wnt signaling. *J. Biol. Chem* .**280**:19883-19887.

12. Veverka V, Henry AJ, Slocombe PM, Ventom A, Mulloy B, Muskett FW, Muzylak M, Greenslade K, Moore A, Zhang L, Gong J, Qian X, Paszty C, Taylor RJ, Robinson MK , and Carr MD (2009) Characterization of the structural features and interactions of sclerostin: molecular insight into a key regulator of Wnt-mediated bone formation. *J .Biol .Chem* .**284**:10890-10900.

13. Poole KE, van Bezooijen RL, Loveridge N, Hamersma H, Papapoulos SE, Löwik CW , and Reeve J (2005) Sclerostin is a delayed secreted product of osteocytes that inhibits bone formation. *FASEB J.* **19**:1842-1844.

14. Silvestrini G, Ballanti P, Leopizzi M, Sebastiani M, Berni S, Di Vito M , and Bonucci E (2007) Effects of intermittent parathyroid hormone (PTH) administration on SOST mRNA and protein in rat bone. *J. Mol. Histol.* **38**:261-269.

15. Van Bezooijen RL, Roelen BA, Visser A, van der Wee-Pals L, de Wilt E, Karperien M, Hamersma H, Papapoulos SE, ten Dijke P , and Löwik CW (2004) Sclerostin is an osteocyte-expressed negative regulator of bone formation, but not a classical BMP antagonist. *J. Exp .Med.* **199**: 805-814.

16. King GJ, Keeling SD , and Wronski TJ (1991) Histomorphometric study of alveolar bone turnover in orthodontic tooth movement. *Bone* **12**: 401-409.

17. Kribbs PJ (1983) Oral findings in osteoporosis. Part 2. Relationship between residual ridge and alveolar bone resorption and generalized skeletal osteopenia. *J. Prosthet Dent.* **50**:719-724.

18. Nishimura I, Hosokawa R , and Atwood DA (1992) The knife-edge tendency in mandibular residual ridges in women. *J .Prosthet Dent.* **67**:820-826.

19. Wowern NV (1981) Micrographic and histomorphometric indices of mandibles for diagnosis of osteopenia. *Scand J. Dent. Res.* **23**:47-63.

20. Wowern NV , and Stoltze K (1979) Comparative bone morphometric analysis of mandibles and 2nd metacarpals. *Scand J .Dent. Res.* **2**:358-364.

21. Yamashiro T , and Takano-Yamamoto T (2001) Influences of ovariectomy on experimental tooth movement in the rats. *J .Dent .Res.* **80**:1858-1861.

22. Elovic RP (1995) Ovariectomy decreased the bone area fraction of the rat mandible. *Calcif .Tissue Int* .**56**: 305-310.

23. Tanaka M, Ejiri S, Nakajima M, Kohno S , and Ozawa H (1999) Changes of cancellous bone mass in rat mandibular condyle following ovariectomy. *Bone* **25**:339-347.

24. Eghbali-Fatourechi G, Khosla S, Sanyal A, Boyle WJ, Lacey DL , and Riggs BL (2003) Role of RANK ligand in mediating increased bone resorption in early postmenopausal women. *J. Clin. Invest.* **111**:1221-1230.

25. Ikeda T, Utsuyama M , and Hirokawa K (2001) Expression profiles of receptor activator of nuclear factor kappaB ligand, receptor activator of nuclear factor kappaB, and osteoprotegerin messenger RNA in aged and ovariectomized rat bones. *J. Bone Miner. Res.* **16**:1416-1425.

26. Yoneda T, Ishimaru N, Arakaki R, Kobayashi M, Izawa T, Moriyama K , and Hayashi Y (2004) Estrogen deficiency accelerates murine autoimmune arthritis associated with receptor activator of nuclear factor-kappa B ligand-mediated osteoclastogenesis. *Endocrinology* **145**:2384-2391.

27. Lacey DL, Timms E, Tan HL, Kelley MJ, Dunstan CR, Burgess T, Elliott R, Colombero A, Elliott G, Scully S, Hsu H, Sullivan J, Hawkins N, Davy E, Capparelli C, Eli A, Qian YX, Kaufman S, Sarosi I, Shalhoub V, Senaldi G, Guo J, Delaney J , and Boyle WJ (1998) Osteoprotegerin ligand is a cytokine that regulates osteoclast differentiation and activation. *Cell* **93**:165-176.

28. Yasuda H, Shima N, Nakagawa N, Yamaguchi K, Kinosaki M, Mochizuki S, Tomoyasu A, Yano K, Goto M, Murakami A, Tsuda E, Morinaga T, Higashio K, Udagawa N, Takahashi N , and Suda T (1998) Osteoclast differentiation factor is a ligand for osteoprotegerin/osteoclastogenesis-inhibitory factor and is identical to TRANCE/RANKL. *Proc. Natl. Acad. Sci. USA* **95**: 3597-3602.

29. Tsukii K, Shima N, Mochizuki S, Yamaguchi K, Kinosaki M, Yano K, Shibata O, Udagawa N, Yasuda H, Suda T , and Higashio K (1998) Osteoclast differentiation factor mediates an essential signal for bone resorption induced by 1 alpha,25-dihydroxyvitamin D3, prostaglandin E2, or parathyroid hormone in the microenvironment of bone. *Biochem. Biophys. Res. Commun.* **246**:337-341.

30. Masuki H, Li M, Hasegawa T, Suzuki R, Ying G, Zhusheng L, Oda K, Yamamoto T, Kawanami M , and Amizuka N (2010) Immunolocalization of DMP1 and sclerostin in the epiphyseal trabecule and diaphyseal cortical bone of osteoprotegerin deficient mice. *Biomed. Res.* **31**: 307-318.

31. Simonet WS, Lacey DL, Dunstan CR, Kelley M, Chang MS, Luthy R, Nguyen HQ, Wooden S, Bennett L, Boone T, Shimamoto G, DeRose M, Elliott R, Colombero A, Tan HL, Trail G, Sullivan J, Davy E, Bucay N, Renshaw-Gegg L, Hughes TM, Hill D, Pattison W, Campbell P, Sander S, Van G, Tarpley J, Derby P, Lee R , and Boyle WJ (1997) Osteoprotegerin: a novel secreted protein involved in the regulation of bone density. *Cell* **89**: 309-319.

32. Ohashi T, Kusuhara S , and Ishida K (1991) Immunoelectron microscopic demonstration of estrogen receptors in osteogenic cells of Japanese quail. *Histochemistry* **96**:41-44.

33. Green S, Walter P , and Greene G (1986) Cloning of the human estrogen-receptor cDNA. *J. Steroid Biochem. Mol. Biol.* **24**:77-83.

34. Kuiper GG, Enmark E, Pelto-Huikko M, Nilsson S , and Gustafsson JA (1996) Cloning of a novel receptor expressed in rat prostate and ovary. *Proc. Natl. Acad. Sci. USA* **11**: 5925-5930.

35. Braidman IP, Davenport LK, Carter DH, Selby PL, Mawer EB , and Freemont AJ (1995) Preliminary in situ identification of estrogen target cells in bone. *J. Bone Miner. Res* .**10**:74-80.

36. Amizuka N, Kwan MY, Goltzman D, Ozawa H, and White JH (1999) Vitamin D3 differentially regulates parathyroid hormone/parathyroid hormone-related peptide receptor expression in bone and cartilage. *J .Clin. Invest* .**103**:373-381.

37. Amizuka N, Yamada M, Watanabe JI, Hoshi K, Fukushi M, Oda K, Ikehara Y , and Ozawa H (1998) Morphological examination of bone synthesis via direct administration of basic fibroblast growth factor into rat bone marrow. *Microsc. Res. Tech.* **15**:313-322.

38. Oda K, Amaya Y, Fukushi-Irie M, Kinameri Y, Ohsuye K, Kubota I, Fujimura S , and Kobayashi J (1999) A general method for rapid purification of soluble versions of glycosylphosphatidylinositol-anchored proteins expressed in insect cells: an application for human tissue-nonspecific alkaline phosphatase. *J. Biochem.* **126**: 694-699.

39. Ubaidus S, Li M, Sultana S, de Freitas PH, Oda K, Maeda T, Takagi R , and Amizuka N (2009) FGF23 is mainly synthesized by osteocytes in the regularly distributed osteocytic lacunar canalicular system established after physiological bone remodeling. *J. Electron Microsc.* **58**:381-392.

40. Freitas de PHL, Li M, Ninomiya T, Nakamura M, Ubaidus S, Oda K, Udagawa N, Maeda T, Takagi R , and Amizuka N (2009) Intermittent PTH administration stimulates

pre-osteoblastic proliferation without leading to enhanced bone formation in osteoclast-less c-fos(-/-) mice. *J. Bone Miner. Res.* **24**:1586-1597.

41. Hasegawa T, Li M, Hara K, Sasaki M, Tabata C, de Freitas PH, Hongo H, Suzuki R, Kobayashi M, Inoue K, Yamamoto T, Oohata N, Oda K, Akiyama Y, and Amizuka N (2011) Morphological assessment of bone mineralization in tibial metaphyses of ascorbic acid-deficient ODS rats. *Biomed. Re.s* **32**: 259-269.

42. Lim SK, Won YJ, Lee HC, Huh KB , and Park YS (1999) A PCR analysis of ER α and β mRNA abundance in rats and the effect of ovariectomy. *J. Bone Miner. Res.* **14**:1189-1196.

43. Krum SA, Miranda-Carboni GA, Hauschka PV, Carroll JS, Lane TF, Freedman LP , and Brown M (2008) Estrogen protects bone by inducing Fas ligand in osteoblasts to regulate osteoclast survival. *EMBO J.* **27**:535-545.

44. Nakamura T, Imai Y, Matsumoto T, Sato S, Takeuchi K, Igarashi K, Harada Y, Azuma Y, Krust A, Yamamoto Y, Nishina H, Takeda S, Takayanagi H, Metzger D, Kanno J, Takaoka K, Martin TJ, Chambon P , and Kato S (2007) Estrogen prevents bone loss via estrogen receptor α and induction of Fas ligand in osteoclasts. *Cell* **130**, 811-823.

FIGURE LEGENDS

Fig. 1 The distribution of TRAP-positive osteoclasts and DMP-1-reactive osteocytes in the interradicular septa of the Sham-operated (Sham) and ovariectomized (OVX) rats

White arrows indicate the direction of mesial and distal regions. The interradicular septum (IRS) of the first molar showed TRAP-positivity (red color), a hallmark of an osteoclast, in the mesial region of Sham-operated specimens **(A)**, while the OVX specimens demonstrated more numerous TRAP-reactivity in the mesial surfaces **(**black arrows, **B)**. The interradicular septa (IRS) of the serial sections showed even distribution of DMP-1 immunoreactivity in the Sham-operated **(C)** and OVX groups **(D)**. Observing the boxed areas in panels **C** and **D** a higher magnification, the intensity of DMP-1 immunoreactive osteocytes was seen throughout the mesial regions of Sham **(E)** and OVX **(F)** groups. Note no obvious difference in the localization of DMP-1-positive osteocytes between the Sham and OVX specimens.

Bar: A-D 250μm, E,F 60μm

Fig. 2 Triple staining of ALP, TRAP and sclerostin in the interradicular septa of the Sham-operated and OVX rats

Panels **C-D** are magnified images of panels **A** and **B**, of which **C, E** and **D, F** show the mesial and distal regions of the Sham and OVX specimens, respectively. At a low magnification, TRAP-reactivity shown in red color was relatively intense in the mesial region of OVX interradicular septum (IRS) **(B)**, compared with the Sham group **(A)**. Brown-colored sclerostin-immunopositivity was seemingly evenly-distributed in the septa of the both groups **(A, B)**. Observing these magnified images, however, Sham-operated specimens showed little sclerostin in osteocytes closely neighboring the mesial surface **(C)**. In contrast, the mesial region of the OVX septa had many osteocytes without the sclerostin-immunoreactivity **(E)**. Please note there were more intense TRAP-positive osteoclasts on the

irregularly-shaped mesial surfaces of the OVX specimens (**E**). The distal regions of both Sham-operated and OVX septa showed no sclerostin-positive osteocytes merely in the superficial layer **(D, F)**. Panel **G** shows a graph representing the percentage of sclerostin-positive osteocytes in each assumed rectangle 30-240μm distant from the mesial surfaces. Please note a low index of sclerostin-positive osteocytes 30 μm distant from surface in the Sham group, while the OVX septa exhibited no sclerostin-positivity in broad area, extending down to 90 μm in depth from the mesial surface.

Bar: A,B 250μm, C-F 60μm

Fig. 3. Immunolocalization of ERα and TUNEL-positive cells in the interradicular septa after OVX

Panels **A-F** demonstrate double staining for ERα/cathepsin K immunoreactivity. ERα-immunoreactivity is shown in brown color, while cathepsin K-positivity is stained in blue. Panels **E** and **F** are magnified images of **A** and **C**, respectively. Panels **A, E** and **C, F** are obtained from the mesial regions, while **B** and **D** show the distal regions of the Sham and OVX groups. In all areas, ERα-immunopositivity was detected in osteoblasts, osteocytes and periodontal cells in the mesial and distal regions of both groups. Please note that not all osteoblasts and osteocytes show ERα-positivity, and also as shown in an inset, cathepsin K-positive osteoclasts (oc) had ERα-reactive nuclei. Panels **G-J** reveal TUNEL distribution in the mesial **(G, I)** and distal **(H, J)** regions of the Sham **(G, H)** and OVX **(I, J)** groups. Insets show higher magnified images of TUNEL-positive cells (blue color). There seems no histological difference in the distribution of TUNEL positive cells after OVX.

PDL: periodontal ligament, **AB:** alveolar bone

Bar: A-D 150μm, E,F 60μm, G-J 30μm

Fig. 4. Distribution of RANKL, TRAP/osteopontin-positive cement lines and osteocytic lacunar-canalicular system in the mesial region of the interradicular septa

Panels **A** and **B** show the immunoreactivity of RANKL in the periodontal ligaments facing the mesial side of the interradicular septum of the Sham and OVX groups, respectively. Please note intense RANKL immunoreactivity (brown color) surrounding TRAP-positive osteoclasts (oc) in the OVX specimens (**B**). Cement lines, a histological hallmark of bone remodeling, were evaluated by TRAP **(C, D)** and osteopontin **(E, F)** histochemistry. There are many TRAP-positive cement lines (arrows) in the OVX specimens (**D**), compared with that in the Sham-operated one **(C)**. Consistently, osteopontin-positive cement lines are numerous in the deeper region of the OVX alveolar bone, than those seen in the Sham group **(E)**. Panels **G** and **H** show silver impregnation in the mesial sides of the interradicular septa of the Sham and OVX groups, when observed under dark field. The Sham-operated specimens show regular distribution of osteocytes (ocy) and their canaliculi (**G**), while OVX bone revealed the irregular distribution of osteocytes (ocy) (**H**).

Bar: A,B 50μm, C-F 100μm, G,H 20μm

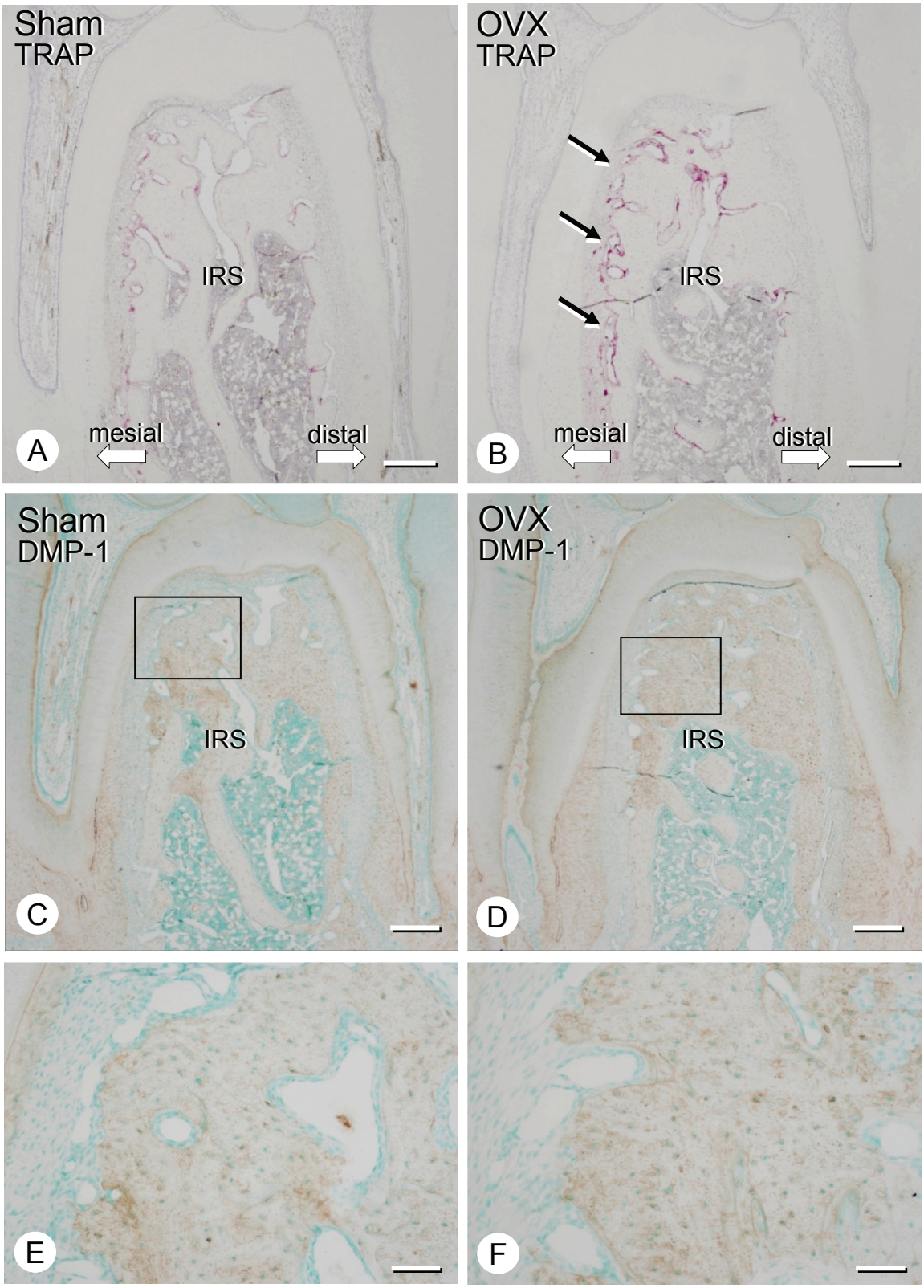
Sham
TRAP
IRS
mesial
distal
A
OVX
TRAP
IRS
mesial
distal
B
Sham
DMP-1
IRS
C
OVX
DMP-1
IRS
D
E
F

Figure 1

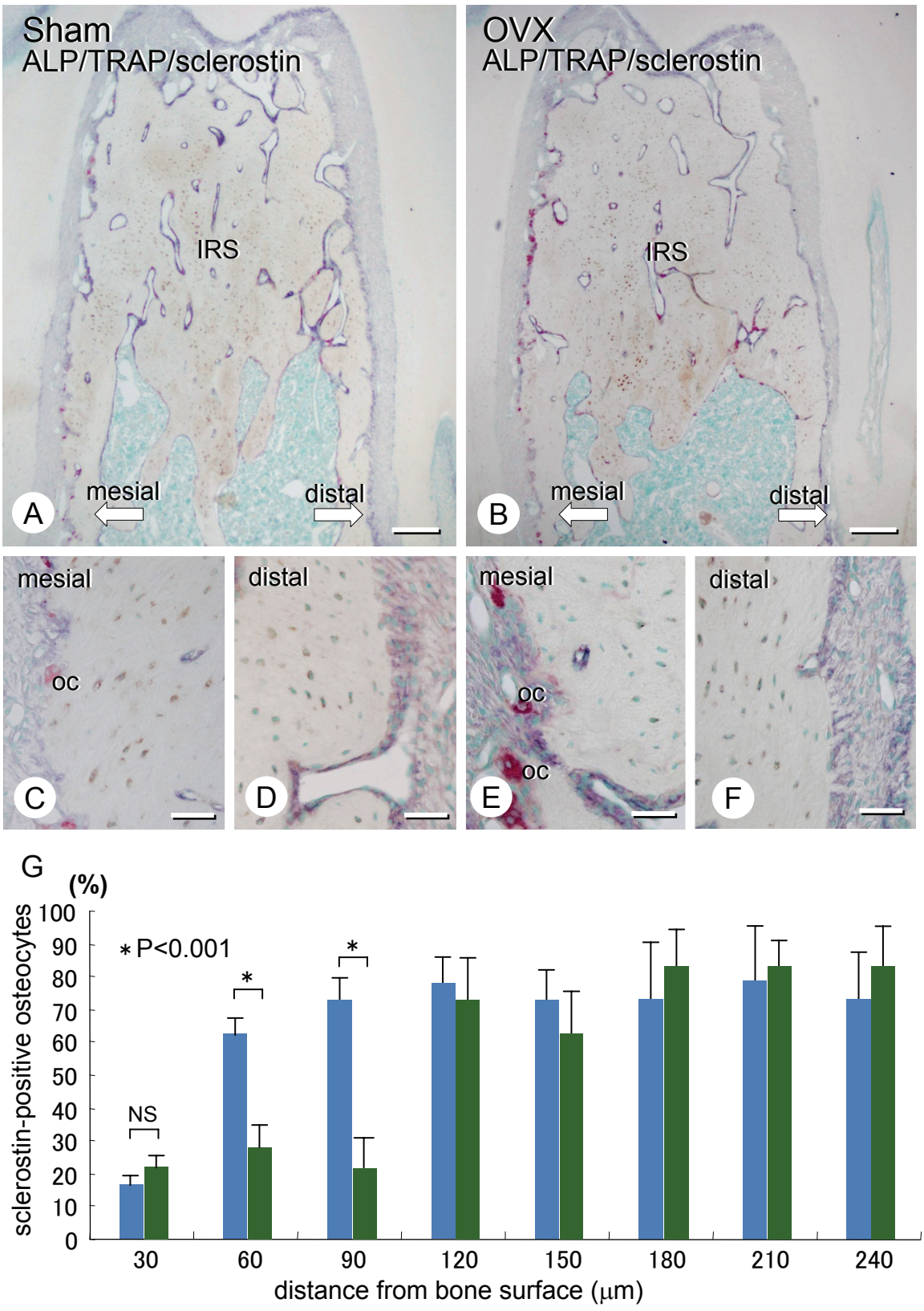
Sham
ALP/TRAP/sclerostin
IRS
mesial
distal
A
OVX
ALP/TRAP/sclerostin
IRS
mesial
distal
B
mesial
oc
C
distal
D
mesial
oc
oc
E
distal
F
G
(%)
sclerostin-positive osteocytes
100
90
80
70
60
50
40
30
20
10
0
＊P<0.001
*
*
NS
30
60
90
120
150
180
210
240
distance from bone surface (μm)

Figure 2

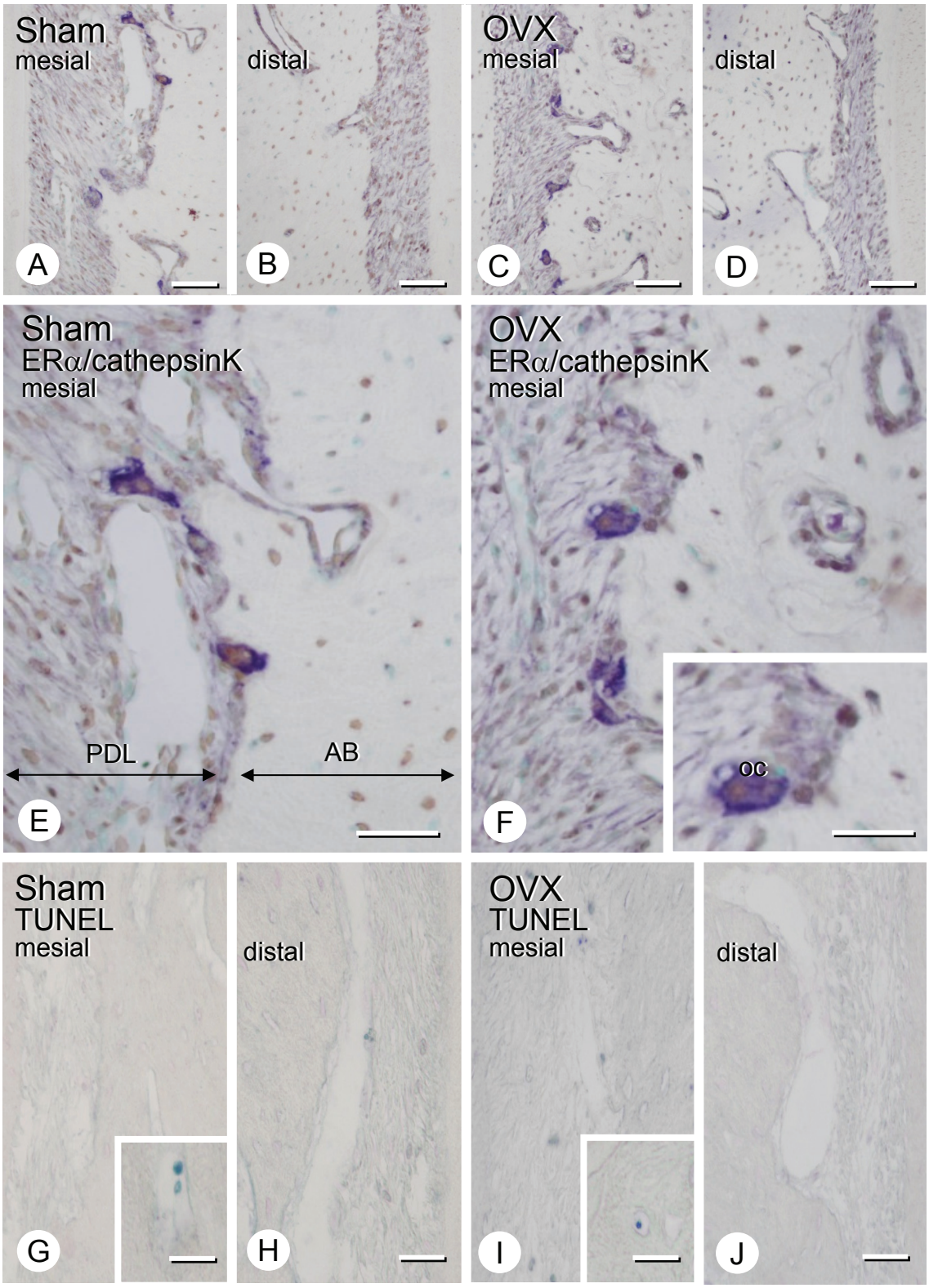
Sham
mesial
distal
OVX
mesial
distal
A
B
C
D
Sham
ERα/cathepsinK
mesial
OVX
ERα/cathepsinK
mesial
PDL
AB
oc
E
F
Sham
TUNEL
mesial
distal
OVX
TUNEL
mesial
distal
G
H
I
J

Figure 3

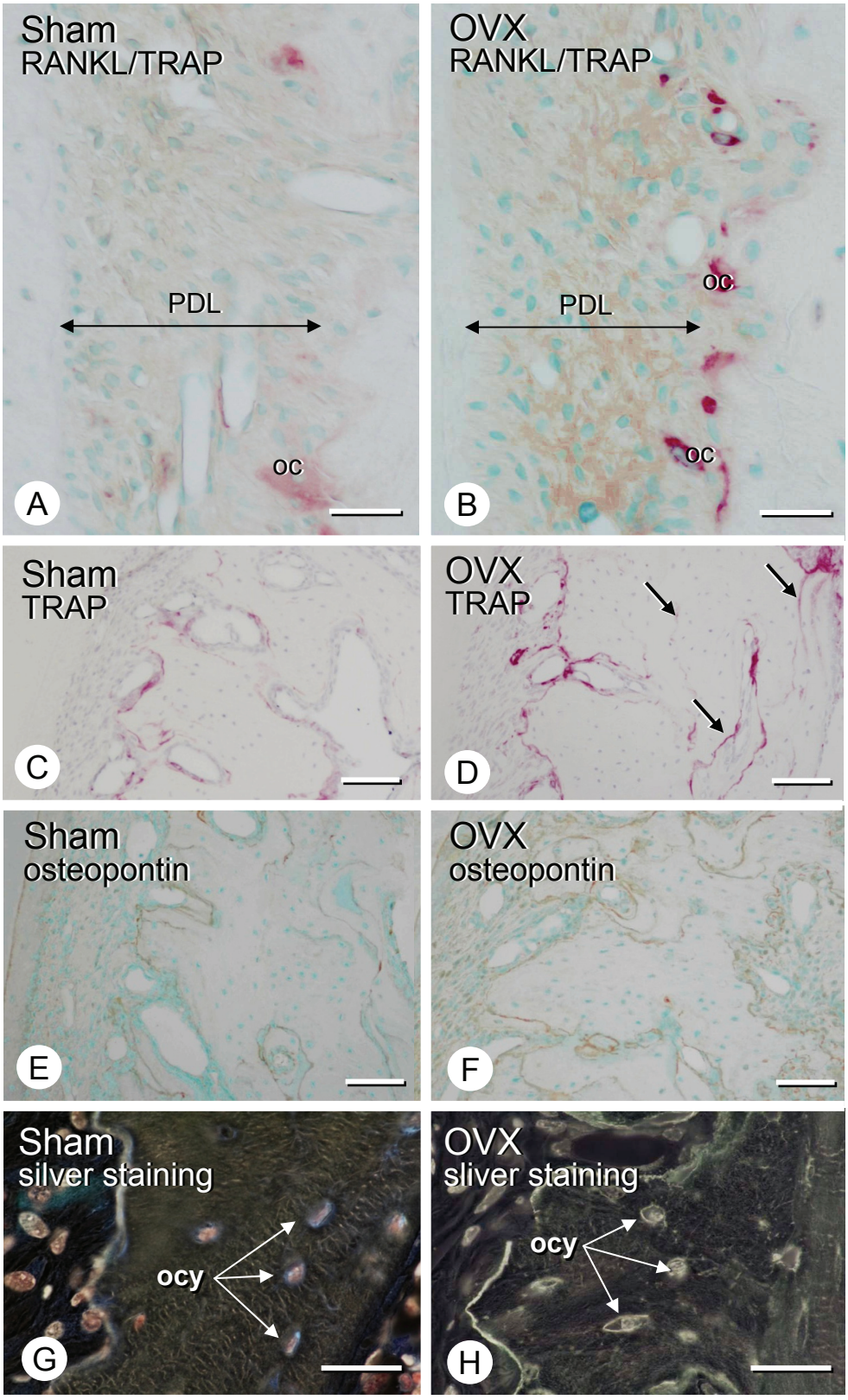
Sham
RANKL/TRAP
PDL
oc
A
OVX
RANKL/TRAP
PDL
oc
oc
B
Sham
TRAP
C
OVX
TRAP
D
Sham
osteopontin
E
OVX
osteopontin
F
Sham
silver staining
ocy
G
OVX
sliver staining
ocy
H

Figure 4